Molecular crowding causes narrowing of population heterogeneity and restricts internal dynamics in a protein

2016 Methods Appl. Fluoresc. 4 014003

(http://iopscience.iop.org/2050-6120/4/1/014003)

Methods and Applications in Fluorescence

PAPER

Molecular crowding causes narrowing of population heterogeneity and restricts internal dynamics in a protein

Samsuzzoha Mondal[1], Mamata V Kallianpur[1], Jayant B Udgaonkar[2] and G Krishnamoorthy[3]

[1] Department of Chemical Sciences, Tata Institute of Fundamental Research, 400005, Mumbai, India
[2] National Centre for Biological Sciences, Tata Institute of Fundamental Research, 565056, Bengaluru, India
[3] Department of Biotechnology, Anna University, 600025, Chennai, India

E-mail: gk@tifr.res.in

RECEIVED
30 June 2015

REVISED
30 August 2015

ACCEPTED FOR PUBLICATION
9 September 2015

PUBLISHED
16 December 2015

Keywords: molecular crowding, intramolecular distance distribution, FRET, side-chain dynamics

Abstract

Macromolecular crowding is a distinguishing property of intracellular media. Knowledge on the structure and dynamics of a protein in a crowded environment is essential for a complete understanding of its function. Reduction in intermolecular space could cause structural and functional alterations. Here, we have studied a model protein barstar to see how polyethylene glycol (PEG)-induced crowding affects its various structural states (native, unfolded and molten-globule-like) with different extents of change in conformational heterogeneity. Intramolecular distances and *distance distributions* were determined by time-resolved Förster resonance energy transfer from Trp53 to several acceptor sites by analysis of fluorescence decay kinetics using the Maximum Entropy Method. We observed PEG-induced narrowing of population distributions along with shifting of populations towards more compact states. Structural compactness also resulted in the slowing down of internal dynamics of the protein as revealed by fluorescence anisotropy decay kinetics of the fluorophore IAEDANS attached at several sites.

1. Introduction

Structure, dynamics and interactions in proteins are conventionally studied in aqueous buffered solutions. However, these media have little resemblance to the cellular environment. The intracellular environment is rather complex due its high content of macromolecules, including carbohydrates, proteins, lipids and nucleic acids. Such a high concentration (up to 400 g l^{-1}) [1, 2] of macromolecules makes the cellular compartments extremely crowded. This is expected to have an impact on the structure, stability and function of proteins [3]. Several specific and non-specific interactions between various macromolecular species make the system extremely complex, and hence, difficult to replicate *in vitro* [4, 5]. A general non-specific effect arising collectively from all macromolecular species is the reduction of intermolecular space which forces every molecule to be confined in a much smaller space compared to in a dilute solution [6, 7]. This effect, known as the 'excluded volume effect', affects the structure and dynamics of macromolecules [1]. The influence of excluded volume can be modelled in *in vitro* experiments by using uncharged polymers like dextrans, polyethyleneglycol (PEG) and Ficoll and small molecules such as trimethylamine N-oxide (TMAO) which are known as 'macromolecular crowding agents' [8, 9]. These popular crowding agents are largely devoid of any specific interactions with proteins, and mimic mainly the excluded volume effect.

Any process resulting in volume change can be biased by the excluded volume effect which pushes the equilibrium towards the state of least volume occupied. Protein folding–unfolding is such a process. The unfolded state of proteins (U-state) has an open and flexible structure compared to that of the native state (N-state) which has a rather compact, and hence less volume-occupying structure [10]. Hence macromolecular crowding can shift the folding–unfolding equilibrium towards the N-state. This is supported by several experimental evidences such as proteins requiring higher temperature or higher denaturant concentration for unfolding in crowded media [8, 11]. However, there are very few studies [12] so far showing how the molecular size gets altered while fitting tight intermolecular spaces. Proteins in their N-state have narrower distribution of conformations due to the rigidness of the native structure. On the other hand, the U-state with its expanded and flexible structure is expected to have a broader distribution of conformations [9, 13].

The extent of conformational heterogeneity can be altered under the influence of macromolecular crowding. In the present study, the major goal is to investigate how protein conformational heterogeneity gets affected by molecular crowding. Motional dynamics of side-chains is expected to be related to conformational heterogeneity. This study also addresses the issue of how motional dynamics of side-chains get altered by molecular crowding.

In the current study, barstar has been chosen as a model protein to study the effect of a crowding agent PEG (average molecular weight 8000) on the native state, the unfolded state and the oligomeric acid state (A-state) of the protein. The A-state is significant because of its similarity with the molten globule state which is usually found to be an obligatory intermediate state between native and unfolded states [14, 15]. Tryptophan fluorescence lifetime has been used as a signature of the conformational state of the single tryptophan mutant protein; the measured lifetime distribution of the ensemble yields an estimate of the heterogeneity of population distribution. As a more direct measure, intramolecular distance distributions have been determined from time resolved Förster resonance energy transfer (FRET) experiments using tryptophan as a donor and 5-thio-2-nitrobenzoic acid (TNB) as an acceptor attached to the single cysteine residue of the mutant barstar. Protein dynamics have also been studied using a 5-((((2-iodoacetyl) amino) ethyl) amino) naphthalene-1-sulfonic acid (1,5-IAEDANS) probe covalently attached to the protein and checked how the local motion of a buried part of the protein gets affected by the external pressure exerted by the crowding agent.

2. Materials and methods

2.1. Chemicals

All the chemicals used were of the highest purity grade available from the commercial sources. 1,5-IAEDANS was from Molecular Probes and DTNB was from Sigma. The native buffer (pH 8.0) was composed of 20 mM Tris–HCl and 250 μM ethylenediaminetetraacetic acid (EDTA). The proteins were unfolded in 5 M guanidine hydrochloride (GdnHCl) solutions in 20 mM Tris–HCl (pH 8.0). For the acid state 20 mM glycine-HCl buffer (pH 2.7) was used. Protein concentration was 15 μM for fluorescence lifetime and anisotropy studies and 50 μM for FRET experiments.

2.2. DTNB labelling of protein

For FRET experiments, single cysteine mutants of barstar containing a single tryptophan (Trp53) were used. Expression and purification of the proteins were done as described previously [16]. Mutant proteins (Cys25, Cys40, Cys62 and Cys82) were labelled with a cysteine attachable fluorescence acceptor 5,5′-dithiobis(2-nitrobenzoic acid) (DTNB). 6 mg of barstar were unfolded using 2.5 mL of 6 M GdnHCl in 100 mM phosphate buffer at pH 8.0, and 6 mM DTNB was added to the unfolded protein. The reaction of DTNB with the cysteine was allowed to proceed for 20 min. The reaction mixture was then passed through a PD10 column (Sephadex G-25, GE Healthcare) pre-equilibrated with 20 mM phosphate buffer, 0.25 mM EDTA at pH 8.0, to remove out the GdnHCl, excess DTNB and the TNB anion released in the reaction of the cysteine with DTNB.

2.3. IAEDANS labelling of protein

Mutant proteins were labeled with a cysteine-specific fluorophore 1,5-IAEDANS after unfolding in 6 M GdnHCl at pH 8. About a 10 to15-fold molar excess of the dye was reacted with the unfolded protein and the labeled protein was separated from free dye and GdnHCl by passing the reaction mixture through a PD-10 column. The extent of labeling was checked by absorbance measurements using a value for ε_{337} of 4500 M^{-1} cm^{-1} at 337 nm for 1,5-IAEDANS.

2.4. Steady state fluorescence measurements and data analysis

Steady state fluorescence measurements were accomplished on a FluoroLog-3 spectrofluorimeter (Horiba Jobin Yvon Inc). Buffer solutions containing varying GdnHCl concentrations were made with and without 20% PEG. Native barstar were then added to the corresponding buffer solutions and fluorescence intensities at 330 nm were measured. Data were analyzed according to the references [17, 18]. Basically, raw fluorescence data at 330 nm were converted to plots of f_{app} versus denaturant concentration using the equation [17, 18],

$$f_{app} = \frac{Y_O - (Y_F + m_F[D])}{(Y_U + m_U[D]) - (Y_F + m_F[D])} \quad (1)$$

Y_O is the observed signal at a particular GdnHCl concentration. Y_F and Y_U represent the intercepts, and m_F and m_U are the slopes of the native and the unfolded baselines, respectively, and were obtained by extrapolation of linear least-squares fits of the baselines. Then, f_{app} values were fit to two-state $F \rightleftarrows U$ unfolding model [17, 18],

$$f_{app} = \frac{\exp[-(\Delta G_U + m_G[D])/RT]}{1 + \exp[-(\Delta G_U + m_G[D])/RT} \quad (2)$$

Where, m_G is the changes in free energy associated to preferential interaction of the denaturant with the unfolded form of the protein relative to the folded form. Mid-point of transition i.e. the denaturant concentration at which the protein is half unfolded at any temperature T, is given by C_m, where $C_m = -\Delta G_U/m_G$.

2.5. Time resolved fluorescence and maximum entropy method (MEM) of data analysis

Time-resolved fluorescence intensity and anisotropy decay measurements were carried out using a time correlated single photon counting setup [19]. For

fluorescence lifetime and TR-FRET measurements, dye-laser pulses at 590 nm frequency-doubled to 295 nm were used for excitation. Emission was collected (at 90° to the excitation beam) at 345 nm for native protein, and at 365 nm for the unfolded and acid states using a 320 nm long pass filter. The instrument response function (IRF) was taken at 295 nm and was found to be 40 ps (FWHM). For all the fluorescence lifetime measurements, peak counts of 20 000 were collected with the emission polarizer oriented at the magic angle (54.7°) with respect to the excitation polarizer. The decay was deconvoluted with respect to IRF and analyzed with maximum entropy method (MEM) [20, 21] of data analysis to obtain the lifetime distribution.

For MEM analysis, the decay curves were fitted with a model equation involving 100 exponentials.

$$I(t) = \sum \alpha_i \exp(-t/\tau_i) \quad i = 1\text{—}100 \qquad (3)$$

$I(t)$ is the fluorescence intensity at time t and α_i is the amplitude of the i-th lifetime τ_i such that $\sum \alpha_i = 1$. The analysis begins by assigning equal probability (amplitude) to all the lifetime values. Subsequently, in each iteration during the analysis, the distribution is modified leading to minimization of χ^2 and maximization of the Shannon–Jaynes entropy function (S),

$$S = -\sum p_i \log p_i \qquad (4)$$

where, $p_i = \alpha_i / \sum \alpha_i$ and α_i is the amplitude of the i-th lifetime.

If many possible distributions have the same or similar values of χ^2, then the maximum entropy criterion selects the distribution for which S is maximum. Thus, MEM analysis results in a lifetime distribution that is independent of any mathematical model.

2.6. Time resolved fluorescence anisotropy decay and data analysis

For all the anisotropy measurements on 1,5-IAEDANS labeled barstar, we used 1 ps pulses of 740 nm radiation of Ti-Sapphire laser. The pulses were frequency doubled to 370 nm to excite the IAEDANS probe and emission were collected at 500 nm in directions parallel ($I_\parallel$) and perpendicular ($I_\perp$) to the polarization of the excitation beam. The anisotropy was calculated as,

$$r(t) = \frac{I_\parallel(t) - I_\perp(t)G(\lambda)}{I_\parallel(t) + 2I_\perp(t)G(\lambda)} \qquad (5)$$

where, $G(\lambda)$ is the geometry factor or G-factor at the wavelength λ of emission. The G-factor of the emission collection optics was determined in separate experiments using a free IAEDANS solution.

Time-resolved anisotropy decay curves were analyzed based on the model,

$$r(t) = r_0 \sum (\beta_1 e^{-t/\varphi_1} + \beta_2 e^{-t/\varphi_2}) \qquad (6)$$

where, r_0 is the initial anisotropy. The values of r_0 for 1,5-IAEDANS is 0.30 ± 0.01 (at λ_{ex} 370 nm) as estimated in independent experiments in 70% glycerol. β_i is the amplitude associated with the i-th rotational correlation time φ_i, such that, $\sum \beta_i = 1$.

2.7. Distance calculation from TR-FRET measurements

The mean donor–acceptor distances (r_{D-A}) of the proteins are calculated from the time dependent FRET studies from the equation,

$$r_{DA} = R_0(\tau_D/\tau_{DA} - 1)^{-1/6} \qquad (7)$$

where, R_0 is the distance between donor and acceptor at which the energy transfer efficiency is 50%, τ_D and $\tau_{D\text{-}A}$ are the donor lifetimes in the absence and presence of the acceptor, respectively.

3. Results and discussion

3.1. Effect of PEG on the stability of barstar

The stability of barstar in presence of 20% PEG was checked by monitoring the unfolding event with increasing concentration of the denaturant guanidine hydrochloride (GdnHCl). 20% PEG is roughly similar to the total concentration of macromolecules in the cytoplasm and hence this concentration was used in several earlier studies [22–24]. The fluorescence intensity of the single buried tryptophan (Trp53) was used to monitor the unfolding. Equilibrium denaturation of barstar with GdnHCl follows a two-state model [17, 18] showing a sigmoidal pattern in fluorescence intensity change with increasing denaturant concentration. In the presence of PEG, the sigmoidal curve gets shifted slightly towards higher concentrations of GdnHCl as observed from the shift of the midpoint of transition (C_m) from 1.48 M to 1.87 M of GdnHCl (figure 1). This indicates marginal stabilization of the protein in the presence of the crowding agent. The protein remains in the unfolded state in 5 M GdnHCl in the presence of 20% PEG.

3.2. Effect of molecular crowding on fluorescence lifetime distribution of Trp53 in native (N), unfolded (U) and acid (A) states

Conformational heterogeneity in different forms (N, U and A) of barstar was monitored through measurement of the fluorescence lifetime distribution of the single tryptophan Trp53. Tryptophan fluorescence lifetime, being quite sensitive to the environment, gives an estimate of the population distribution of conformational states [10, 25]. The model-free approach, maximum entropy method (MEM, see 'Materials and Methods') was used to generate the lifetime distribution (figure 2). The presence of PEG (20%) was found to result in a significant reduction in the width of the lifetime distribution, for all the three states (figure 2 and table 1). Thus, it can be inferred that macromolecular crowding results in narrowing the population distribution in all cases. The effect is more pronounced in the U and A-forms compared to in the N state, consistent with their higher levels of structural

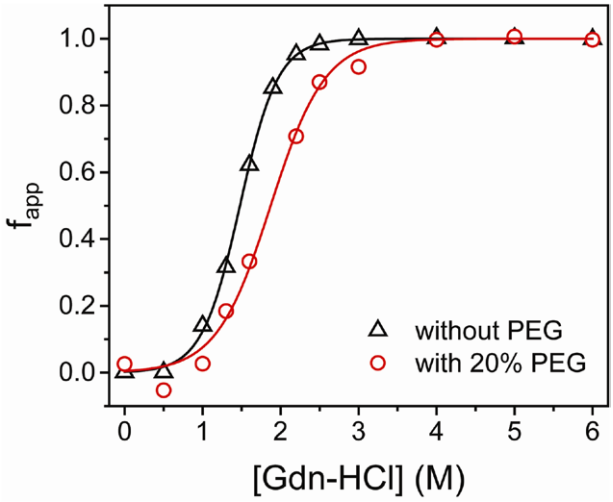

Figure 1. Equilibrium denaturation curves of barstar at 25 °C, pH 8. Raw fluorescence intensities at 330 nm are converted to f_{app} values using equation (1), and are plotted against GdnHCl concentration. The solid lines through the data are nonlinear least-squares fits of the data according to equation (2) and yield values for m_G and C_m of -2.42 ± 0.1 kcal.mol^{-1} M^{-1} and 1.48 ± 0.1 M in the absence of PEG, and -1.70 ± 0.1 kcal.mol^{-1} M^{-1} and 1.87 ± 0.2 M in the presence of 20% PEG respectively.

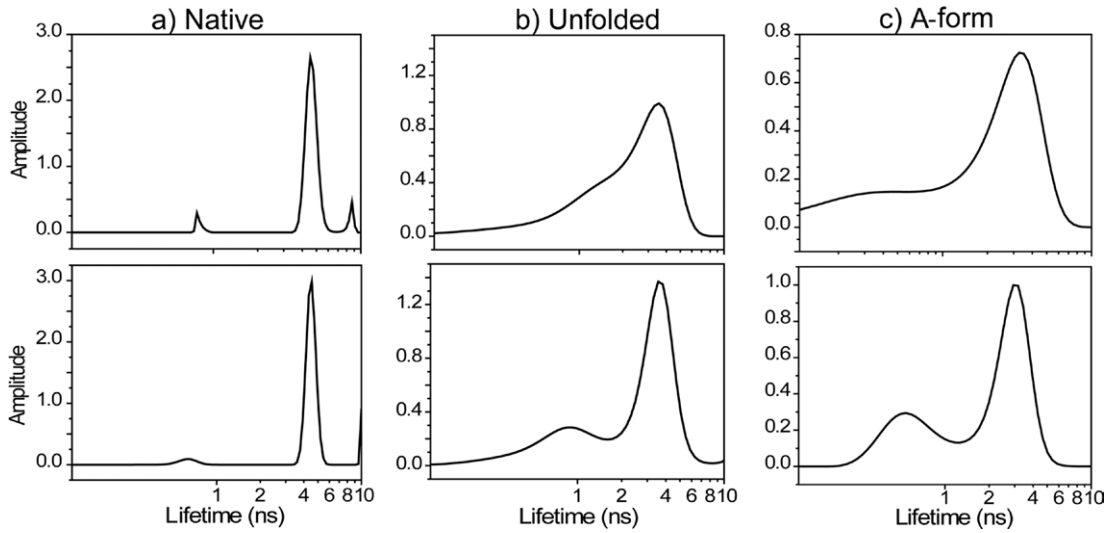

Figure 2. Tryptophan fluorescence lifetime distribution in the absence (top) and in the presence of 20% PEG (bottom) in (a) native (20 mM tris-HCl, pH 8.0), (b) unfolded (20 mM tris-HCl, 5 M GdnHCl, pH 8.0) and (c) A-forms (20 mM glycine-HCl, pH 2.7) of barstar respectively.

Table 1. Width and peak values (τ_{max}) obtained from MEM analysis of tryptophan fluorescence lifetime distribution (figure 2).

	Width (ns)[a]		Peak value (τ_{max}, ns)[b]	
Sample	w/o PEG	With PEG	w/o PEG	With PEG
Native	1.93 ± 0.06	1.90 ± 0.30	4.91 ± 0.10	5.04 ± 0.08
Unfolded	2.35 ± 0.60	1.35 ± 0.20	3.19 ± 0.05	3.61 ± 0.03
A-form	2.60 ± 0.09	1.50 ± 0.20	3.31 ± 0.06	3.09 ± 0.03

[a] Width has been calculated from the Gaussian fit of the distribution curve.

[b] τ_{max} values are obtained from the position of the major peak in the lifetime distributions.

flexibility when compared to the N-state. Furthermore, a small shift in the populations towards longer lifetimes was observed in the cases of N and U, and towards the shorter lifetime region in the case of the A-form (figure 2 and table 1).

Although structural interpretation of a change in the fluorescence lifetime (in the absence of a well-identified non-radiative process) can be ambiguous, the observed changes do indicate a PEG-induced change in the environment of Trp53. The PEG-induced shift in the peak of lifetime distribution towards the longer lifetimes suggests that Trp53 gets more buried, especially in the U form as a result of the external pressure caused by the crowding agent (table 1). It is important to note that the protein remains in the U form in 5 M GdnHCl and PEG, as shown in the melting curves (figure 1). Hence the observed change

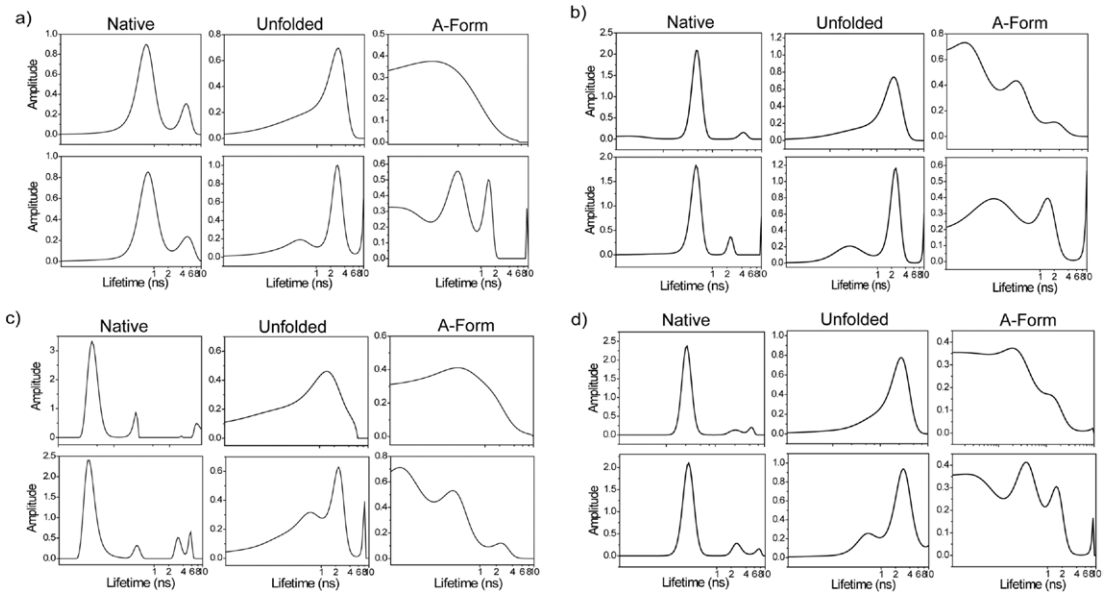

Figure 3. Tryptophan fluorescence lifetime distributions of TNB (FRET acceptor)-labeled barstar mutant variants—(a) Cys25-TNB; (b) Cys40-TNB; (c) Cys62-TNB and (d) Cys82-TNB in the native (20 mM tris-HCl, pH 8.0), unfolded (20mM tris-HCl, 5 M GdnHCl, pH 8.0) and A-forms (20 mM glycine-HCl, pH 2.7). The top panels represent the distribution in the absence of PEG, and the bottom panels represent the same in the presence of 20% PEG.

Table 2. Widths and peak values of fluorescence lifetime distributions and mean donor- acceptor distances (r_{D-A}) estimated from FRET between Trp53 and TNB.

		Width (ns)[a]		τ_{D-A} (ns)[b]			r_{D-A} (Å)[d]	
Sample	State	w/o PEG	with PEG	w/o PEG	with PEG	R_0 (Å)[c]	w/o PEG	with PEG
	N	0.53 ± 0.03	0.68 ± 0.10	0.69 ± 0.01	0.76 ± 0.01	26.9	19.9 ± 0.1	20.2 ± 0.1
Cys25-TNB	U	2.39 ± 0.07	1.45 ± 0.06	2.85 ± 0.02	2.79 ± 0.02	22.5	32.1 ± 0.1	27.6 ± 0.1
	A	–	–	0.43 ± 0.04	0.37 ± 0.04	22.6	18.1 ± 0.3	17.4 ± 0.3
	N	0.22 ± 0.01	0.20 ± 0.01	0.46 ± 0.01	0.43 ± 0.01	25.2	17.3 ± 0.1	17.0 ± 0.1
Cys40-TNB	U	1.99 ± 0.10	1.17 ± 0.08	2.26 ± 0.05	2.42 ± 0.05	22.6	26.2 ± 0.1	25.4 ± 0.1
	A	–	–	0.24 ± 0.01	0.46 ± 0.01	22.6	16.2 ± 0.1	18.2 ± 0.1
	N	0.01 ± 0.01	0.02 ± 0.01	0.04 ± 0.01	0.04 ± 0.02	26.8	12.0 ± 0.5	12.0 ± 1.0
Cys62-TNB	U	1.58 ± 0.30	1.55 ± 0.10	1.42 ± 0.09	2.22 ± 0.10	22.6	21.8 ± 0.2	24.4 ± 0.2
	A	–	–	0.48 ± 0.02	0.29 ± 0.03	22.6	18.6 ± 0.2	16.6 ± 0.3
	N	0.11 ± 0.02	0.13 ± 0.01	0.27 ± 0.01	0.27 ± 0.01	27.0	16.8 ± 0.1	16.7 ± 0.1
Cys82-TNB	U	2.73 ± 0.08	1.98 ± 0.03	2.85 ± 0.03	3.09 ± 0.01	22.7	32.4 ± 0.1	30.6 ± 0.1
	A	–	–	0.28 ± 0.02	0.35 ± 0.04	22.7	16.7 ± 0.2	17.3 ± 0.3

[a] Widths are calculated from the Gaussian fits of lifetime distributions.

[b] For N and U-forms τ_{D-A} and τ_D values are taken from the peak maxima of the lifetime distributions (figures 2 and 3). For the A-form, average τ_{D-A} and τ_D values are calculated using the equation, $\tau_{avg} = \sum \alpha_i \tau_i / \sum \alpha_i$. Thus, in absence of PEG, τ_D is 2.04 ± 0.06 ns and in presence of PEG it is 2.14 ± 0.03 ns for the A-forms.

[c] R_0 values are taken from elsewhere [16].

[d] Distances (r_{D-A}) are calculated from the equation (7).

in the fluorescence lifetime distribution comes purely form the U state and not from a mixture of N and U states. However, the A form shows the opposite behavior wherein Trp53 gets more solvent exposed in the presence of PEG which might seem counter-intuitive. The A-form is an aggregate of ~ 16 monomers [26] and hence the aggregation level itself could be sensitive to crowding.

3.3. Effect of macromolecular crowding on intramolecular distance and its distribution

The effect of crowding on average structure and structural distribution can be better revealed from intramolecular distance and distance distributions obtained from FRET experiments. A single cysteine residue engineered at various sites was coupled to a thiol-specific fluorescence-silent acceptor of

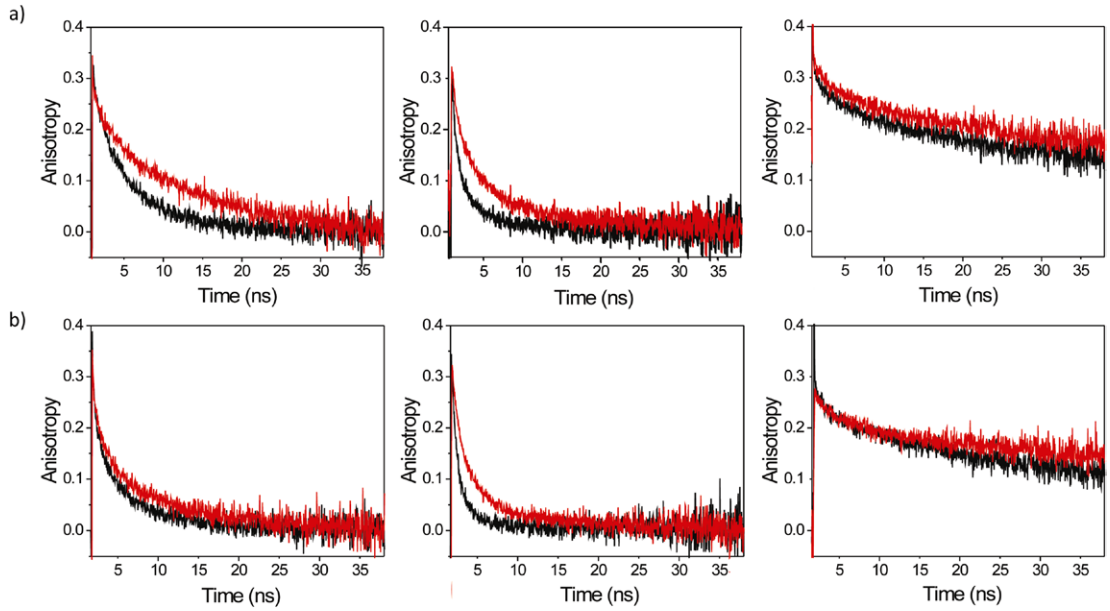

Figure 4. 1,5-IAEDANS fluorescence anisotropy decays for the N, U and A forms of barstar where 1,5-IAEDANS is attached to either Cys40 (a) or Cys82 (b) in the absence (black) and presence (red) of 20% PEG. Rotational correlation times estimated from these decay profiles are given in table 3.

tryptophan fluorescence, 5,5'-dithiobis(2-nitrobenzoic acid) (DTNB) [27]. We used four different mutant variants of barstar which have a single tryptophan (Trp53) along with a single cysteine residue at four different positions (25, 40, 62 and 82) and calculated distances from Trp53-TNB time-resolved FRET, using the Förster equation (equation (7)).

Unlike the case of fluorescence lifetime distribution of Trp53 in the unlabeled protein (figure 2 and table 1), lifetime distributions obtained in the TNB-labeled proteins are controlled by FRET and hence the peak values and the widths of lifetime distribution (figure 3 and table 2) provide us a clear read-out of the intramolecular distances and distance distribution. The native state did not show any significant PEG-induced change in the width of distribution or in the four intramolecular distances again as expected for a compact small protein. However, the U state showed significant PEG-induced reduction in the width of lifetime distribution for all the 4 mutant proteins (figure 3 and table 2). The smaller reduction seen in the case of Cys62 could be the result of the shorter intramolecular distance in this case (table 2). Furthermore, it is noted that the width is the smallest in this case indicating a low level of structural heterogeneity of this short segment even in the absence of the crowding agent. The width of the distribution could not be estimated reliably for the A-form due to the presence of multiple peaks (figure 3).

Intramolecular distances in the N state (table 2) estimated from the peak positions of lifetime distributions obtained in the absence and presence of TNB (figures 2 and 3) agree with those obtained from the NMR structure [16, 28]. Intramolecular distances in the U-form derived from the peak positions also agree with earlier estimates [29]. In the presence of PEG, these distances decrease for three of the four mutant variants (25, 40 and 82) in their U-forms indicating PEG-induced compaction of the U-form. Similar observations have been made in recent studies on the ribosomal protein S16 [30]. The PEG-induced increase in the W53–C62 distance observed for the U-form is beyond experimental error. This observation is unique and requires further investigation. The native states did not show significant reduction in intramolecular distances, as expected. However, the A-form behaved in a non-uniform manner i.e. reduction was seen for two mutant proteins (25, 62) but increase for the other two (40, 82). This could be the result of the aggregated nature of the A-form. In aggregates, fluorescence of the donor in a peptide could be quenched by the acceptor group belonging to another peptide apart from quenching within the same peptide. In this situation, the change in FRET efficiency may not represent the change in the intramolecular distance within a peptide chain.

3.4. Effect of PEG on motional dynamics of sidechains

In order to address the question whether the motional dynamics of sidechains gets affected by the effect of macromolecular crowding, fluorescence anisotropy decay kinetics of a thiol-specific fluorophore, 1,5-IAEDANS attached to the single cysteine sidechain of the mutant proteins was monitored. Cys40 and Cys82, where the cysteine residues have the least surface accessibilities (solvent-accessibility is 5% for Cys40 and 20% for Cys82) [16] were selected for these studies.

Fluorescence anisotropy decay profiles show decrease in the rates in the presence of PEG for all the samples (figure 4). Decay profiles were fitted to a model

Table 3. Parameters associated with fluorescence anisotropy decay in IAEDANS-labelled single cysteine-containing mutants of barstar.

Cys40-IAEDANS	φ_1 (ns)	β_1	φ_2 (ns)	β_2	Cys82-IAEDANS	φ_1 (ns)	β_1	φ_2 (ns)	β_2
N	1.00 ± 0.20	0.19	5.00 ± 0.20	0.81	N	0.48 ± 0.09	0.59	4.06 ± 0.20	0.41
N + PEG	1.12 ± 0.30	0.25	11.7 ± 0.6	0.75	N + PEG	0.90 ± 0.10	0.49	7.8 ± 1	0.51
U	0.65 ± 0.04	0.57	3.40 ± 0.30	0.43	U	0.45 ± 0.05	0.63	2.11 ± 0.07	0.37
U + PEG	1.40 ± 0.10	0.52	8 ± 1	0.48	U + PEG	1.40 ± 0.10	0.71	8.50 ± 0.40	0.29
A	2.30 ± 0.20	0.22	52 ± 3	0.78	A	2.00 ± 0.40	0.17	50 ± 5	0.83
A + PEG	2.20 ± 0.40	0.18	60 ± 10	0.82	A + PEG	1.50 ± 0.10	0.16	72 ± 5	0.84

with two rotational correlational times using equation (6). The faster rotational correlation time (φ_1) represents the local motional freedom of the probe with respect to the polypeptide chain and the slower correlation time (φ_2) represents the global tumbling dynamics of the entire protein [29].

The longer correlation time (φ_2) which represents the global tumbling dynamics increases in the presence of PEG in all the cases. This could be a general effect caused by the increase in viscosity. The acid form showed a very long rotational correlation time (>50 ns) consistent with its large size as the protein forms aggregate in this state (pH < 3) [13, 15]. The correlation time associated with global tumbling dynamics is expected to be independent of the location of the probe. $\varphi_2 \sim 5$ ns observed at Cys40 agrees with the tumbling dynamics of the protein of 10 kD. However, 4.1 ns observed for Cys82 should represent a combination of global tumbling dynamics and unresolved segmental dynamics around Cys82.

Apart from φ_2 which behaved as expected, the shorter correlation time (φ_1) associated with a combination of local motions at Cys40 and Cys82 and motions of polypeptide gets dampened in the N-state and the U-forms (table 3). Firstly, it is noted that, in the N state, the rate of this dynamics is quite slow even in the absence of PEG. Local (or internal) dynamics of sidechains on the surface of protein structure is generally in the range of 0.1–0.3 ns [31, 32]. Significantly longer values of φ_1 viz. 0.48 ns (for Cys82-IAEDANS) and 1.0 ns (for Cys40-IAEDANS) observed in the N-state, could be due the partially buried nature of Cys82 and Cys40 (20% and 5% solvent accessibility [16]) apart from possible contributions from segmental dynamics of the local polypeptide chain. This makes the observation of PEG-induced dampening of local the dynamics unusual and interesting. That the sidechains which are mostly solvent-inaccessible feel the presence of PEG in the medium implies that the molecular crowding exerts external pressure on the protein and this gets transduced to the interior of the protein. Since dynamics, apart from structure, has been recognized as an important factor controlling function [33, 34], knowledge on internal dynamics and their site-specific variation under intracellular conditions becomes an essential parameter in understanding molecular interactions in cells.

4. Conclusions

In this work, we have estimated the effect of macromolecular crowding by PEG on the structure and dynamics of the small protein barstar. Tryptophan fluorescence lifetime distributions, along with the donor–acceptor distance distributions in FRET experiments, revealed a decrease in structural heterogeneity in the unfolded protein. The decrease in the average intramolecular distances which was observed under crowding, in the case of unfolded protein, shows that the unfolded peptide moves towards a more compact structure. From fluorescence anisotropy decay observations we have found that crowding also affects the dynamics of sidechains having low accessibility to solvent. Such crowding-induced changes in structure and dynamics are expected to cause changes in the activity of proteins in the cellular environment.

Acknowledgments

The authors acknowledge financial support from Tata Institute of Fundamental Research, Government of India. Note: The funders had no role in study design, data collection and analysis, decision to publish, or preparation of the manuscript.

Competing interests

The authors have declared that no competing interests exist.

References

[1] Minton A P 2001 The influence of macromolecular crowding and macromolecular confinement on biochemical reactions in physiological media *J. Biol. Chem.* **276** 10577–80
[2] Sarkar M, Smith A E and Pielak G J 2013 Impact of reconstituted cytosol on protein stability *Proc. Natl Acad. Sci.* **110** 19342–7
[3] Fulton A B 1982 How crowded is the cytoplasm *Cell* **30** 345–7
[4] Ellis R J and Minton A P 2003 Cell biology—join the crowd *Nature* **425** 27–8
[5] van den Berg B, Ellis R J and Dobson C M 1999 Effects of macromolecular crowding on protein folding and aggregation *Embo J.* **18** 6927–33
[6] Minton A P and Wilf J 1981 Effect of macromolecular crowding upon the structure and function of an enzyme:

glyceraldehyde-3-phosphate dehydrogenase *Biochemistry* **20** 4821–6
[7] Mikaelsson T, Aden J, Johansson L B A and Wittung-Stafshede P 2013 Direct observation of protein unfolded state compaction in the presence of macromolecular crowding *Biophys. J.* **104** 694–704
[8] Sasahara K, McPhie P and Minton A P 2003 Effect of dextran on protein stability and conformation attributed to macromolecular crowding *J. Mol. Biol.* **326** 1227–37
[9] Homouz D, Sanabria H, Waxham M N and Cheung M S 2009 Modulation of calmodulin plasticity by the effect of macromolecular crowding *J. Mol. Biol.* **391** 933–43
[10] Saxena A, Udgaonkar J B and Krishnamoorthy G 2005 Protein dynamics and protein folding dynamics revealed by time-resolved fluorescence *Fluorescence Spectroscopy in Biology* vol 3 (Berlin: Springer) pp 163–79
[11] Samiotakis A, Wittung-Stafshede P and Cheung M S 2009 Folding, stability and shape of proteins in crowded environments: experimental and computational approaches *Int. J. Mol. Sci.* **10** 572–88
[12] Dhar A, Samiotakis A, Ebbinghaus S, Nienhaus L, Homouz D, Gruebele M and Cheung M S 2010 Structure, function, and folding of phosphoglycerate kinase are strongly perturbed by macromolecular crowding *Proc. Natl Acad. Sci. USA* **107** 17586–91
[13] Krishnamoorthy G 2012 Motional dynamics in proteins and nucleic acids control their function: revelation by time-domain fluorescence *Curr. Sci.* **102** 266–76
[14] Khurana R and Udgaonkar J B 1994 Equilibrium unfolding studies of barstar—evidence for an alternative conformation which resembles a molten globule *Biochemistry* **33** 106–15
[15] Jha A, Udgaonkar J B and Krishnamoorthy G 2009 Characterization of the heterogeneity and specificity of interpolypeptide interactions in amyloid protofibrils by measurement of site-specific fluorescence anisotropy decay kinetics *J. Mol. Biol.* **393** 735–52
[16] Sridevi K and Udgaonkar J B 2003 Surface expansion is independent of and occurs faster than core solvation during the unfolding of barstar *Biochemistry* **42** 1551–63
[17] Agashe V R and Udgaonkar J B 1995 Thermodynamics of denaturation of barstar—evidence for cold denaturation and evaluation of the interaction with guanidine-hydrochloride *Biochemistry* **34** 3286–99
[18] Nath U and Udgaonkar J B 1997 Folding of tryptophan mutants of barstar: evidence for an initial hydrophobic collapse on the folding pathway *Biochemistry* **36** 8602–10
[19] Narayan S, Kombrabail M H, Das S, Singh H, Chary K V R, Rao B J and Krishnamoorthy G 2015 Site-specific fluorescence dynamics in an rna 'thermometer' reveals the role of ribosome binding in its temperature-sensitive switch function *Nucleic Acids Res.* **43** 493–503
[20] Swaminathan R and Periasamy N 1996 Analysis of fluorescence decay by the maximum entropy method: influence of noise and analysis parameters on the width of the distribution of lifetimes *Proc. Indian Acad. Sci.* **108** 39–49
[21] Brochon J C 1994 Maximum entropy method of data analysis in time-resolved spectroscopy *Methods Enzymol.* **240** 262
[22] Kidoaki S and Yoshikawa K 1999 Folding and unfolding of a giant duplex-DNA in a mixed solution with polycations, polyanions and crowding neutral polymers *Biophys. Chem.* **76** 133–43
[23] Sasaki Y, Miyoshi D and Sugimoto N 2007 Regulation of DNA nucleases by molecular crowding *Nucleic Acids Res.* **35** 4086–93
[24] Zhou H-X, Rivas G and Minton A P 2008 Macromolecular crowding and confinement: biochemical, biophysical, and potential physiological consequences *Annu. Rev. Biophys.* **37** 375
[25] Swaminathan R, Krishnamoorthy G and Periasamy N 1994 Similarity of fluorescence lifetime distributions for single tryptophan proteins in the random coil state *Biophys. J.* **67** 2013
[26] Juneja J, Bhavesh N S, Udgaonkar J B and Hosur R V 2002 Nmr identification and characterization of the flexible regions in the 160 kda molten globule-like aggregate of barstar at low ph *Biochemistry* **41** 9885–99
[27] Ramachandran S and Udgaonkar J B 1996 Stabilization of barstar by chemical modification of the buried cysteines *Biochemistry* **35** 8776–85
[28] Lubienski M J, Bycroft M, Freund S M V and Fersht A R 1994 3D solution structure and c-13 assignments of barstar using nuclear-magnetic-resonance spectroscopy *Biochemistry* **33** 8866–77
[29] Saxena A M, Udgaonkar J B and Krishnamoorthy G 2006 Characterization of intra-molecular distances and site-specific dynamics in chemically unfolded barstar: evidence for denaturant-dependent non-random structure *J. Mol. Biol.* **359** 174–89
[30] Mikaelsson T, Ådén J, Johansson L B-Å and Wittung-Stafshede P 2013 Direct observation of protein unfolded state compaction in the presence of macromolecular crowding *Biophys. J.* **104** 694–704
[31] Mukhopadhyay S, Nayak P K, Udgaonkar J B and Krishnamoorthy G 2006 Characterization of the formation of amyloid protofibrils from barstar by mapping residue-specific fluorescence dynamics *J. Mol. Biol.* **358** 935–42
[32] Lakshmikanth G S and Krishnamoorthy G 1999 Solvent-exposed tryptophans probe the dynamics at protein surfaces *Biophys. J.* **77** 1100–6
[33] Henzler-Wildman K A, Lei M, Thai V, Kerns S J, Karplus M and Kern D 2007 A hierarchy of timescales in protein dynamics is linked to enzyme catalysis *Nature* **450** 913–27
[34] Daniel R M, Dunn R V, Finney J L and Smith J C 2003 The role of dynamics in enzyme activity *Annu. Rev. Biophys. Biomol. Struct.* **32** 69–92